System based on the contrast of Purkinje images to measure corneal and lens scattering

PAU SANTOS,[1] JUAN A. MARTÍNEZ-RODA,[1] JUAN C. ONDATEGUI,[1] FERNANDO DÍAZ-DOUTÓN,[1] JORGE A. ORTIZ CAZAL,[2] AND MERITXELL VILASECA[1,*]

[1]*Center for Sensors, Instruments and Systems Development (CD6), Universitat Politècnica de Catalunya (UPC), Rambla Sant Nebridi 10, Terrassa 08222, Barcelona, Spain*
[2]*Hospital CIMA Sanitas, Passeig Manuel Girona 33, Barcelona 08034, Barcelona, Spain*
*meritxell.vilaseca@upc.edu

Abstract: Current methods to measure intraocular scattering provide information on the total scattered light, which consists of the combined contributions originating from different ocular structures. In this work, we propose a technique for the objective and independent assessment of scattering caused by the cornea and the lens based on the analysis of the contrast of the third and fourth Purkinje images. The technique is preliminarily validated first by using artificial eyes with different levels of corneal and lens scattering; second, it is validated in eyes wearing customized contact lenses to simulate corneal scattering and eyes with nuclear cataracts. Finally, it is tested on a larger population of eyes with cataracts and corneal disorders to prove its clinical usefulness.

References and links

1. D. P. Piñero, D. Ortiz, and J. L. Alio, "Ocular scattering," Optom. Vis. Sci. **87**(9), E682–E696 (2010).
2. J. A. Martínez-Roda, M. Vilaseca, J. C. Ondategui, M. Aguirre, and J. Pujol, "Effects of aging on optical quality and visual function," Clin. Exp. Optom. **99**(6), 518–525 (2016).
3. J. C. Ondategui, M. Vilaseca, M. Arjona, A. Montasell, G. Cardona, J. L. Güell, and J. Pujol, "Optical quality after myopic photorefractive keratectomy and laser in situ keratomileusis: Comparison using a double-pass system," J. Cataract Refract. Surg. **38**(1), 16–27 (2012).
4. P. Artal, A. Benito, G. M. Pérez, E. Alcón, A. De Casas, J. Pujol, and J. M. Marín, "An objective scatter index based on double-pass retinal images of a point source to classify cataracts," PLoS One **6**(2), e16823 (2011).
5. L. T. Chylack, Jr., J. K. Wolfe, D. M. Singer, M. C. Leske, M. A. Bullimore, I. L. Bailey, J. Friend, D. McCarthy, and S. Y. Wu, "The Lens Opacities Classification System III," Arch. Ophthalmol. **111**(6), 831–836 (1993).
6. M. A. Vivino, S. Chintalagiri, B. Trus, and M. Datiles, "Development of a Scheimpflug slit lamp camera system for quantitative densitometric analysis," Eye (Lond.) **7**(Pt 6), 791–798 (1993).
7. L. Franssen, J. E. Coppens, and T. J. T. P. van den Berg, "Compensation comparison method for assessment of retinal straylight," Invest. Ophthalmol. Vis. Sci. **47**(2), 768–776 (2006).
8. T. J. T. P. van den Berg and J. K. Ijspeert, "Clinical assessment of intraocular stray light," Appl. Opt. **31**(19), 3694–3696 (1992).
9. G. Łabuz, F. Vargas-Martín, T. J. T. P. van den Berg, and N. López-Gil, "Method for in vitro assessment of straylight from intraocular lenses," Biomed. Opt. Express **6**(11), 4457–4464 (2015).
10. F. Díaz-Doutón, A. Benito, J. Pujol, M. Arjona, J. L. Güell, and P. Artal, "Comparison of the retinal image quality with a Hartmann-Shack wavefront sensor and a double-pass instrument," Invest. Ophthalmol. Vis. Sci. **47**(4), 1710–1716 (2006).
11. M. Vilaseca, M. J. Romero, M. Arjona, S. O. Luque, J. C. Ondategui, A. Salvador, J. L. Güell, P. Artal, and J. Pujol, "Grading nuclear, cortical and posterior subcapsular cataracts using an objective scatter index measured with a double-pass system," Br. J. Ophthalmol. **96**(9), 1204–1210 (2012).
12. D. Christaras, H. Ginis, A. Pennos, and P. Artal, "Scattering contribution to the double-pass PSF using Monte Carlo simulations," Ophthalmic Physiol. Opt. **37**(3), 342–346 (2017).
13. H. Ginis, O. Sahin, A. Pennos, and P. Artal, "Compact optical integration instrument to measure intraocular straylight," Biomed. Opt. Express **5**(9), 3036–3041 (2014).

14. A. Pennos, H. Ginis, A. Arias, D. Christaras, and P. Artal, "Performance of a differential contrast sensitivity method to measure intraocular scattering," Biomed. Opt. Express **8**(3), 1382–1389 (2017).
15. J. M. Bueno, D. De Brouwere, H. Ginis, I. Sgouros, and P. Artal, "Purkinje imaging system to measure anterior segment scattering in the human eye," Opt. Lett. **32**(23), 3447–3449 (2007).
16. T. J. T. P. van den Berg, L. Franssen, and J. E. Coppens, "Straylight in the human eye: testing objectivity and optical character of the psychophysical measurement," Ophthalmic Physiol. Opt. **29**(3), 345–350 (2009).
17. ISO 15004–2:2007 "Ophthalmic instruments–Fundamental requirements and test methods–Part 2: Light hazard protection."
18. P. A. Barrionuevo, E. M. Colombo, M. Vilaseca, J. Pujol, and L. A. Issolio, "Comparison between an objective and a psychophysical method for the evaluation of intraocular light scattering," J. Opt. Soc. Am. A **29**(7), 1293–1299 (2012).
19. G. C. de Wit, L. Franssen, J. E. Coppens, and T. J. T. P. van den Berg, "Simulating the straylight effects of cataracts," J. Cataract Refract. Surg. **32**(2), 294–300 (2006).
20. M. Bahrami, M. Hoshino, B. Pierscionek, N. Yagi, J. Regini, and K. Uesugi, "Optical properties of the lens: an explanation for the zones of discontinuity," Exp. Eye Res. **124**, 93–99 (2014).
21. A. de Castro, A. Benito, S. Manzanera, J. Mompeán, B. Cañizares, D. Martínez, J. M. Marín, I. Grulkowski, and P. Artal, "Three-dimensional cataract crystalline lens imaging with swept-source optical coherence tomography," Invest. Ophthalmol. Vis. Sci. **59**(2), 897–903 (2018).
22. R. Navarro, J. A. Méndez-Morales, and J. Santamaría, "Optical quality of the eye lens surfaces from roughness and diffusion measurements," J. Opt. Soc. Am. A **3**(2), 228–234 (1986).

1. Introduction

Scattering due to disturbances in the optical media causes some photons entering the human eye to reach previously sheltered retinal locations [1]. Intraocular scattering, which is low in young eyes, becomes significant with age [2], laser refractive surgery [3] and diseases such as cataracts [4].

The Lens Opacities Classification System III (LOCS III) [5] was created in 1993 to clinically grade cataracts from a set of colored slit-lamp and retroillumination photographs, with the aim to minimize the intrinsic variability attributable to the examiner. In order to improve the assessment of intraocular scattering, Vivino et al. [6] developed a Scheimpflug camera for quantitative densitometric applications of ocular structures; this system was used to correlate optical density with cataract grade. To improve upon the clinical applicability of "direct compensation" [8], Franssen et al. [7] proposed a "two alternatives forced choice" psychophysical method called "compensation comparison". In the former, a ring shaped glare source produced straylight on a dark background test field due to the scattering of light by ocular structures, which was sequentially compared with the luminance of a stimulus in the same test region. With the use of "compensation comparison", a central test field is subdivided in two half fields (one with and one without counterphase compensation light) and the subject must decide which one flickers more strongly [9].

Other authors have reported objective approaches for the assessment of intraocular scattering such as the double pass (DP) technique [10,11], in which a 2-mm laser beam is focused onto the retina (first pass), and from the retina it is then reflected to a camera (second pass). Since the first pass is limited by diffraction, the DP image provides information on the ocular point spread function (PSF). This technique frequently uses near-infrared light for patient comfort, although it penetrates into deeper retinal layers from which it is diffused back [12]. Ginis et al. [13,14] proposed the use of extended light sources and green light, which is less affected by fundus diffusion, to enhance sensitivity and as a result enabling the measurement of scattered light at angles up to 7 degrees and avoiding the impact of aberrations in the central part of the PSF. In their attempt to remove the fundus contribution from the assessment of intraocular scattering, Bueno et al. [15] developed a Purkinje-based system. They registered the fourth Purkinje image (the reflex of the back surface of the lens) of a collimated beam and analyzed the light distribution in saturated and unsaturated conditions.

All these technologies provide information on the total ocular scatter, which consists of the combined contributions originating from the different ocular components. In this work, we propose a novel technique based on recording and analyzing the contrast of the third and

fourth Purkinje images (the reflexes of the first and second surfaces of the lens) for the objective and independent assessment of scattering caused by different parts of the eye. We hypothesize that the third Purkinje image is affected by light scattered in the cornea and in the anterior chamber, whereas the fourth Purkinje image is additionally affected by scattering produced inside the lens.

2. Methods and materials

2.1 Purkinje imaging system and contrast computation

Figure 1 shows the layout of the Purkinje system developed. It consists of a xenon lamp (XL) (Hamamatsu Photonics, Hamamatsu, Japan) whose light is projected towards an opaque plate (OP) with 2 slits (3mm x 5mm) to create images with a structured pattern of light with 2 vertical fringes and a central dark fringe of the same size. Although instruments such as the C-Quant often use circular patterns with a central disk and a peripheral annulus to account for scattering, the use of a 1-dimensional configuration with a slit width of 3 mm allowed avoiding overlap of Purkinje images, while, at the same time, not having diffraction effects. To facilitate centering, especially of the third and the fourth Purkinje images, we added two extra horizontal slits to the external parts of the stimulus (top and bottom). However, only the two vertical slits were used to measure scattering. A long-pass filter with a cutoff wavelength of 760 nm (F1) (IR-76, Edmund Optics, New Jersey, USA) that allows near-infrared pass while blocking visible light, thus avoiding pupil contraction, was placed between XL and OP. The stimulus was placed at a distance of 90 mm from the eye in order to obtain a glare source subtending an angle larger than 1° as suggested in the literature when dealing with the ocular PSF [16]. The Purkinje images of the 2-fringes pattern were recorded with a 14-bits electron multiplying CCD (EMCCD) camera (Luca, Andor Technology, Belfast, UK). A telecentric objective (TO) lens (MVTC23024, Thorlabs GmbH, Munich, Germany) was used to minimize distortion and increase the depth of field for all images to be acquired with one single shot exposure. A blue light emitting diode (LED) (M470F3, Thorlabs GmbH, Munich, Germany) emitting at 470 nm was used as a fixation target (FT). An additional filter with the same features as F1 (F2) was placed in front of TO to avoid blue light from the FT reaching the camera. The use of this configuration prevented overlap of the Purkinje images, although overlap also depends on the angle between the stimulus and the visual axis (40°) and between the visual axis and the camera (20°). Finally, a stepper motor was used (ST2818M1006-A, Nanotec, Feldkirchen, Germany) to control the distance between the system and the eye. The setup was mounted on a breadboard so that the system could be moved as a whole. Finally, we enclosed it inside a black box, and a chinrest and a couple of 3-D printed grab bars were added for patient comfort and to minimize movement during measurements (Fig. 2). The system complied with ISO 15004-2:2007 [17], which regulates the requirements of ophthalmic instruments for light hazard protection.
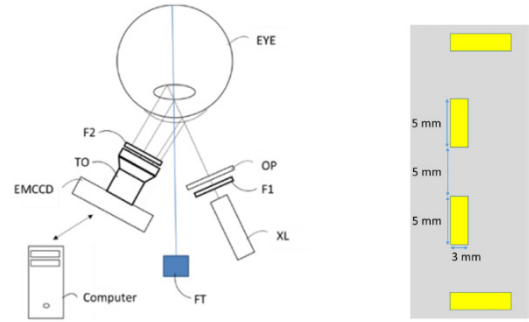
Fig. 1. (Left) Layout of the Purkinje system. XL: xenon lamp; F1, F2: long-pass filters; OP: opaque plate with 2-fringe pattern; TO: telecentric objective lens; EMCCD: electron multiplying CCD; FT: fixation target. (Right) Schematic of the 2-fringes pattern stimulus.

Figure 3 shows the Purkinje images obtained with the system using an artificial eye model and the vertical intensity profile of the fourth Purkinje image. Because the first Purkinje image (P1) is much brighter than the others, it becomes saturated when the dynamic range of the camera is optimized to record the other three. P1 and P2 overlap due to the scarce thickness of the cornea. To compute the intensity profile of the third and fourth images, we manually selected a sufficiently big region of interest (ROI) to include one isolated Purkinje image (see yellow rectangle in Fig. 3); the intensity profile was then calculated as the maximum pixel value for each row inside the ROI: the first value of the intensity profile corresponded to the maximum value along the first row inside the ROI, the second value of the intensity profile corresponded to the maximum value of the second row inside the same area, and so forth.
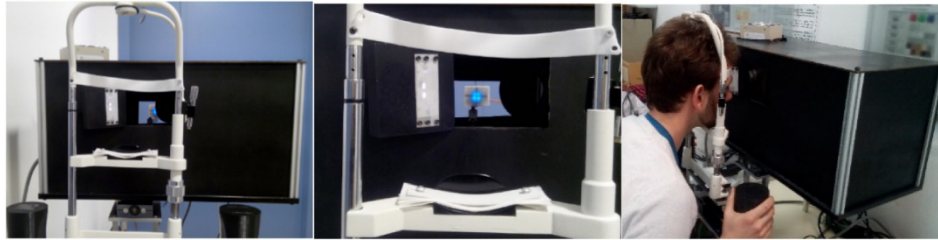

Fig. 2. Several views of the system showing the stimulus (white) and fixation target (blue).
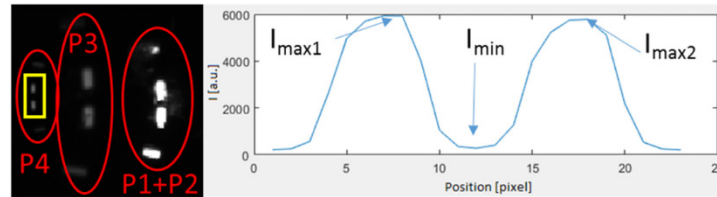

Fig. 3. (Left) Four Purkinje images of an artificial eye. The yellow rectangle is the ROI selected to compute the intensity profile of the fourth image. (Right) Intensity profile of the fourth Purkinje image in arbitrary units [a. u.].

Two contrast values were computed for the third and fourth Purkinje images as follows:

$$Contrast_i = \frac{I_{maxi} - I_{min}}{I_{maxi} + I_{min}}, i = 1\, and\, 2 \qquad (1)$$

where I_{max} and I_{min} are the two maximum intensities and the minimum intensity of the profile, respectively. The greater the scattered light, the higher the I_{min} with respect to I_{max}; consequently, the contrast decreases as scattering increases. For an ideal system free from scattering, I_{min} would be 0, and therefore the contrast of 1.

A contrast value for each Purkinje image (P3 and P4) was finally calculated as the average of $Contrast_1$ and $Contrast_2$.

2.2 Preliminary validation I: measurements with artificial eye models

We firstly tested the proposed methodology on artificial eyes. We used the commercial model OEMI-7 (Ocular Instruments Inc., Bellevue, WA, USA), which is a compact eye model with sizes, radii and refractive indexes similar to the human eye; and a customized model that consisted of a cornea from the Eyetech Laser Eye Model LE-110 (Eyetech Ltd., Morton Grove, Ill., USA), and a couple of concentric plano-convex lenses ACL2520U and ACL1512U (Thorlabs GmbH, Munich, Germany) attached to one another by their planar surfaces to emulate the human lens. We printed a holder with the Witbox 2 3D printer (BQ, Madrid, Spain) to place the cornea and lens at the desired positions (Fig. 4).

Commercial filters were used to simulate different amounts of corneal and lens scattering. We used the filter Cinegel 3020 (c3020) (Rosco, Stamford, USA), with properties similar to a mature cataract [18]; and the filters Black Pro Mist 1 (BPM1) and Black Pro Mist 4 (BPM4) (Tiffen, NY, USA), with optical characteristics that mimic low amounts of scattering and an early cataract, respectively [19]. With the OEMI-7 model, 5 levels of corneal scattering were simulated by placing the following filters in front of the eye: (1) no filter (naked); (2) BPM1; (3) BPM4; (4) one single sheet of the c3020 filter; (5) and two sheets of the c3020 filter placed together (double). In the case of the customized eye model, we simulated lens scattering by placing the filters between the 2 plano-convex lenses. Three different levels of scattering were achieved: (1) no filter (naked); (2) one sheet of the c3020; (3) and two sheets of the c3020 (double). Three repeated measurements were performed for all conditions.

Fig. 4. (Left) Artificial eye OEMI-7. (Right) Front and top view of the customized eye model.

2.3 Preliminary validation II: in-vivo measurements

Four healthy eyes of 4 subjects aged 24 ± 3 years wearing scatter-customized contact lenses (CLs) to simulate different levels of corneal opacification were included in the study. Customized versions of the commercial *Cataract* CL (9mm SFX, Tucson, USA) were used. According to the manufacturer, the CLs presented the following scattering values: 5%, 15% and 50%. We measured the naked eyes of the volunteers and also their eyes wearing CLs with the following degrees of scatter: low (L), medium (M), high (H) and very high (VH); L corresponded to 5%, M to 15%, H to 5% plus 15%, and VH to 15% plus 15%. We also tried CLs with scattering values of 50% and over, but they were too opaque. Sixteen eyes of 16 patients aged 58 ± 8 years with healthy corneas and different grades of nuclear cataracts classified as NO1 (7), NO2 (5), and NO3 (4) (nuclear opalescence in the LOCS III) were also enrolled in the study to account for lens scattering. Five eyes of healthy subjects were used as control group (age: 40 ± 10 years).

The protocol throughout the study included the assessment of intraocular scattering using the Purkinje imaging system (P3 and P4 contrasts) and the following parameters: the

Objective Scatter Index (OSI) measured with the DP-based system HD Analyzer (Visiometrics S.L., Cerdanyola, Spain); the Log(S) from the C-Quant straylight meter based on the compensation comparison method (C-Quant, Oculus Optikgeräte GmbH, Germany); and the densitometry from the Pentacam Scheimpflug camera (Oculus, Lynwood, WA, USA). Three repeated measurements were performed for all eyes. The studies were conducted at the University Vision Center - CUV (Terrassa, Spain) and Hospital CIMA Sanitas (Barcelona, Spain) under the supervision of 3 ophthalmologists (J.C, S.S. and L.C.). After receiving a written and verbal explanation on the nature of the study, all patients provided written informed consent before any examination, and ethical committee approval was obtained. The study followed the tenets of the Declaration of Helsinki (as revised in Tokyo in 2004).

2.4 Clinical validation on a larger population of cataracts and eyes with corneal disorders

To prove its usefulness, a final validation of the methodology was carried out on a larger population of cataracts and eyes with corneal disorders that were not included in the preliminary tests. In this case, 46 eyes of 46 patients (age: 56.4 ± 10.0 years) with different grades of nuclear cataracts (30) and predominantly nuclear cataracts (16) were included in the analysis: from NO1 to NO3 (nuclear opalescence) and from C1 to C2 (cortical cataracts) or P1 to P2 (posterior subcapsular cataracts). Furthermore, 11 eyes from 11 patients (age: 38.8 ± 12.2 years) with corneal disorders such as keratitis, cornea Verticillata, and Fuchs dystrophy were also included as well as post-LASIK patients with any loss of corneal transparency (haze etc.). In this case, twenty-five eyes of healthy subjects were used as control group (age: 45.6 ± 11.6 years). The protocol followed throughout this study was the same as the one used in the preliminary validation.

3. Results

Figure 5 shows the acquired Purkinje images for the OEMI-7 and customized artificial eyes, for the naked eye and using the c3020 filter. As expected, the higher the scattering, the lower the P3 and P4 contrasts. Figure 6 depicts the P3 and P4 contrasts obtained with the OEMI-7 eye model for different levels of corneal scattering and with the customized artificial eye for different levels of lenticular scattering.
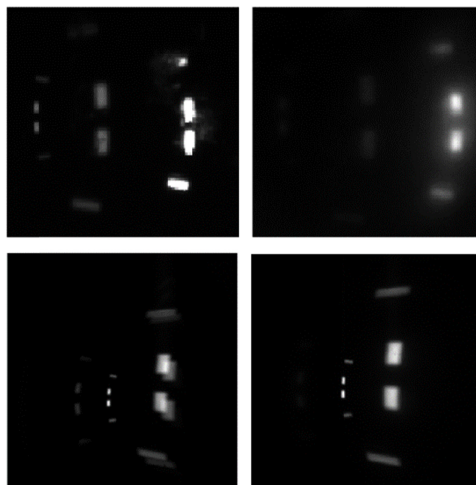

Fig. 5. Purkinje images for the naked OEMI-7 eye (top left) and with one single sheet of the c3020 filter (top right). The same images for the customized artificial eye (bottom). In the customized artificial eye a tilt was introduced to separate the reflexes of the planar surfaces of the plano-convex lenses and the other Purkinje images. These reflexes can be seen on the right of the images while P1 + P2 were not registered in this specific case.
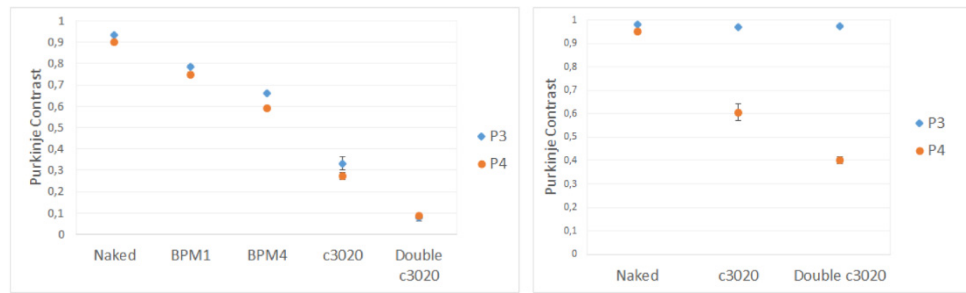
Fig. 6. P3 and P4 contrasts obtained with the OEMI-7 eye model for different levels of corneal scattering (left), and with the customized artificial eye for different levels of lens scattering (right). Error bars are the standard deviation of the mean (SD) of 3 consecutive measurements. Contrasts corresponding to c3020 and double c3020 are different in the left and right plots as different eye models were used to simulate corneal and lens scattering.

Figure 7 depicts the boxplots of the results corresponding to preliminary in-vivo measurements of eyes wearing scatter-customized CLs. Densitometry is not shown since all eyes had values of 100 (saturated). P3 and P4 contrasts decreased as scattering increased, while the straylight in terms of Log(S) increased. Larger OSI values were found for higher scattering conditions, although those labeled as H and VH were linked to more variability. We should underscore that both conditions corresponded to eyes wearing two CLs simultaneously; misalignments and heterogeneous tear distribution between CLs can probably introduce aberrations that affect the central part of the PSF and consequently, the OSI. It should be noted that for one of the volunteers the P3 contrast could not be measured when simultaneously wearing two CL, since the intensity was too low.
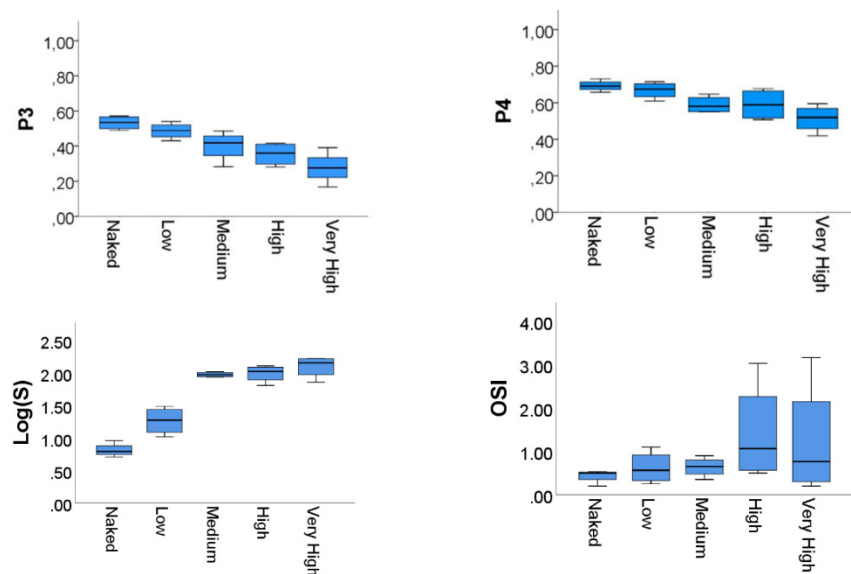

Fig. 7. Scattering outcomes for different levels of corneal scattering simulated with CLs. The dark line in the middle is the median, the top and bottom of the box are the third and first quartiles. The T-bars extend to 1.5 times the height of the box or, if no case has a value in that range, to the minimum or maximum. Each box is based on 12 observations (4 observers, 3 times each), except in the case of the P3 contrast, for which only 3 observers were available.

Correlation coefficients between pairs of variables are summarized in Table 1. Results indicated that significant correlations existed between all pairs of variables except for the OSI and P3 contrast.

Table 1. Correlation coefficients (p-value) between pairs of variables for eyes wearing scatter-customized CLs. Pearson's† and Spearman's‡ values are used for normal and non-normal distributions of data, respectively.

	P3 contrast	P4 contrast	OSI
P4 contrast	0.828† (<.001)*	-	
OSI	−0.340‡ (0.154)	−0.491‡ (0.028)*	-
Log(S)	−0.830‡ (<.001)*	−0.810‡ (<.001)*	0.511‡ (0.021)*

*Statistically significant correlations.

Figure 8 shows the boxplots of the measured scattering as a function of cataract severity (LOCS III) for eyes with cataracts included in the in-vivo preliminary validation. We found agreement between cataract grade and all techniques used. We also analyzed correlations between pairs of variables (Table 2). Unexpectedly, results suggested that all pairs of variables were correlated, including the P3 contrast, which means that to some extent it is also affected by cataracts.
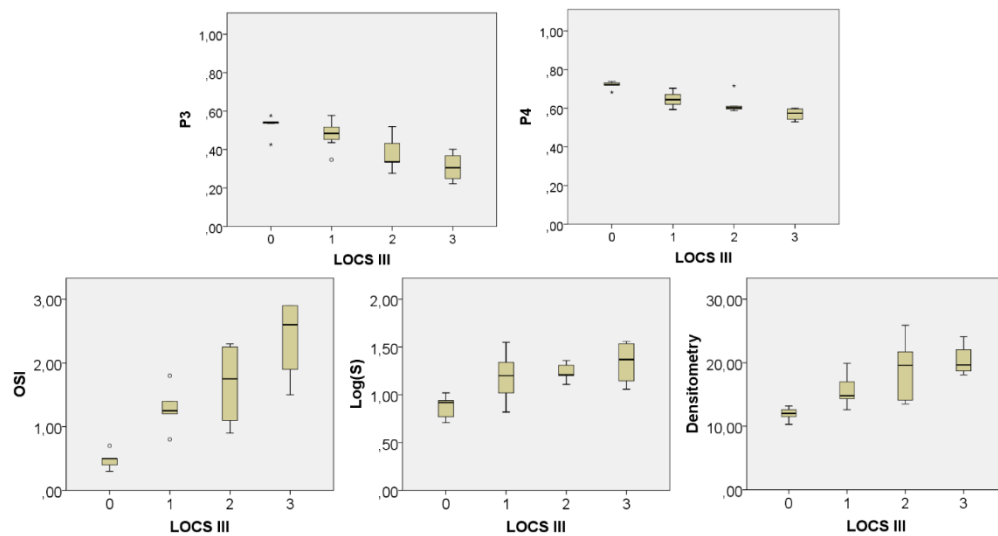
Fig. 8. Scattering outcomes as a function of the LOCS III classification for eyes included in the in-vivo preliminary validation: NO1(1), NO2(2), and NO3(3); and control group (0). The dark line in the middle is the median, the top and bottom of the box are the third and first quartiles. The T-bars extend to 1.5 times the height of the box or, if no case has a value in that range, to the minimum or maximum. The points are outliers. Boxes are based on 15 (0), 21 (1), 15 (2), and 12 (3) observations (5, 7, 5, and 4 observers, 3 times each).

Table 2. Correlation coefficients (p-value) between pairs of variables for eyes with cataracts included in the preliminary validation. Since variables were normally distributed, Pearson's values are shown.

	P3 contrast	P4 contrast	OSI	Log(S)
P4 contrast	0.844 (<.001)*	-		
OSI	−0.733 (<.001)*	−0.761 (<.001)*	-	
Log(S)	−0.682 (0.001)*	−0.630 (<.001)*	0.615 (0.005)*	-
Densitometry	−0.726 (<.001)*	−0.787 (<.001)*	0.631 (0.004)*	0.546 (<.010)*

*Statistically significant correlation.

A detailed analysis of the Purkinje images in eyes with cataracts included in the preliminary validation revealed that in 9 of the 16 cases a Ghost Purkinje Image (GPI) appeared next to P3 affecting its contrast computation (Fig. 9). Figure 10 (left) depicts the P3 contrast as a function of the GPI maximum intensity (GPI_{max}), as well as the corresponding linear fitting: $P3 = a \cdot GPI_{max} + b$. It is apparent that P3 is notably influenced by the GPI light distribution. In order to remove the lens backscattered light from the computed P3 contrast, we corrected the raw P3 as shown in Eq. (2).

$$P3^{'} = P3 - a \cdot (GPI_{max}) \tag{2}$$

For the sake of completeness, Fig. 10 (right) shows the linear regression between P3′ and P4. While no significant correlations were found between them for eyes with cataracts, the correlation was significant for eyes with induced corneal scattering (CLs). Unlike P3, P3′ did not show any trend with respect to the LOCS III classification (Fig. 11).
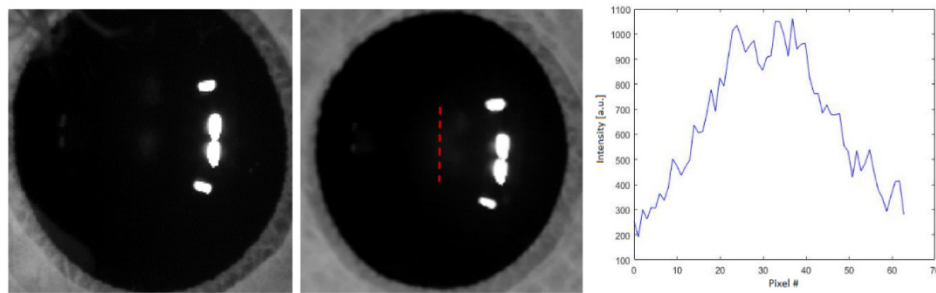

Fig. 9. Purkinje images from an eye without (left) and with (middle) GPI. Intensity profile of the GPI corresponding to the red dashed line in arbitrary units [a. u.] (right). The maximum value of this profile is used to correct the P3 contrast.
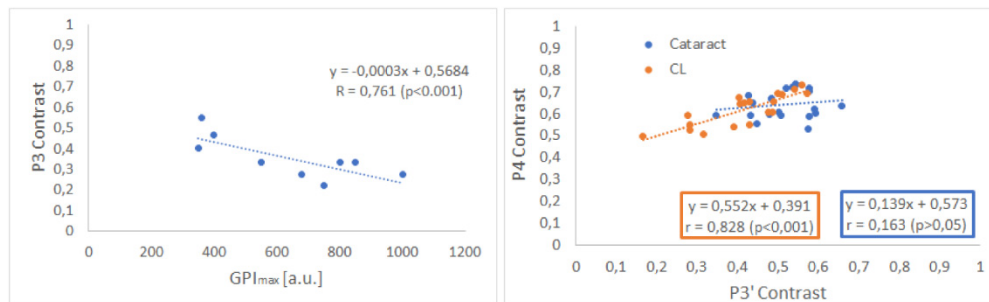

Fig. 10. P3 contrast vs. GPI_{max} for eyes with GPI (left) and P4 vs. corrected P3′ contrast (right). Eyes with cataracts in blue and eyes wearing scatter-customized CLs in orange.
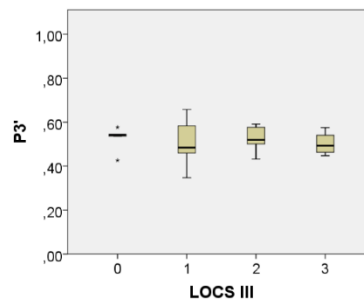
Fig. 11. P3′ contrast as a function of the LOCS III classification: NO1(1), NO2(2), and NO3(3); and control group (0). The dark line in the middle is the median, the top and bottom of the box are the third and first quartiles. The T-bars extend to 1.5 times the height of the box or, if no case has a value in that range, to the minimum or maximum. The points are outliers.

Figure 12 shows the results of applying the proposed technique on the larger population of eyes, i. e., healthy eyes (25), eyes with cataracts (46) and with corneal disorders (11). The results of eyes wearing customized CLs are also shown for comparison. P3 is higher in eyes of the control group, proving that cataracts have an influence on P3. A t-test confirmed that there were significant differences between the control and cataract groups ($p<0.001$), and the control and CLs groups ($p = 0.005$); in contrast, no differences were found between cataracts and eyes with CLs and between cataracts and eyes with corneal disorders ($p>0.05$). Nevertheless, P3′ showed similar values for eyes with healthy corneas (control and cataract groups) ($p>0.05$), whereas significant differences were reported between the CLs group and the other two (control and cataract groups) ($p<0.001$), and between eyes with corneal disorders and the other two ($p<0.001$). Finally, P4 showed differences between healthy eyes and eyes with scattering (cornea or lens) ($p<0.001$), but not between the cataract and CLs groups and between cataracts and eyes with corneal disorders ($p>0.05$).
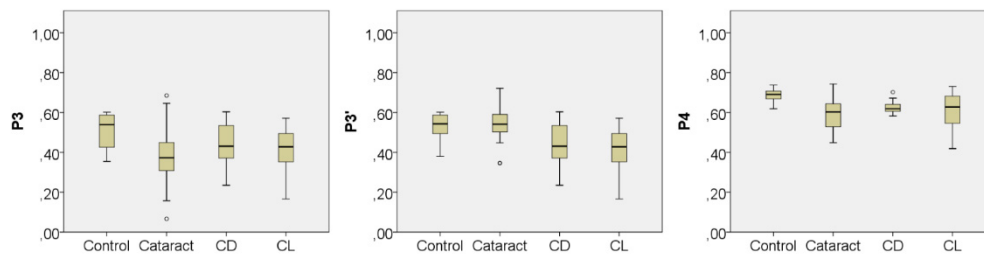

Fig. 12. Boxplots showing P3 (left), P3′ (middle) and P4 (right) contrasts for eyes of the control group (25), with cataracts (45), with corneal disorders (CD) (11) and eyes wearing scatter-customized CLs. The dark line in the middle is the median, the top and bottom of the box are the third and first quartiles. The T-bars extend to 1.5 times the height of the box or, if no case has a value in that range, to the minimum or maximum. The points are outliers.

4. Discussion

The technique based on the analysis of the contrast of the third and fourth Purkinje images described in this study provides an objective and independent assessment of scattering caused by the cornea (and the anterior chamber) and the lens. Although Bueno et al. [15] also used a Purkinje imaging system to measure anterior segment scattering in the human eye, which was firstly tested in an artificial eye and later in normal young eyes wearing customized CLs, they only registered the P4 image of a collimated beam and analyzed the light distribution in saturated and unsaturated conditions to compute the parameter of Scattering (POS). POS was based on the areas under the radial profiles of the images and was sensitive enough to discriminate different induced levels of intraocular scattering, avoiding the contribution from

the retina. Unlike this system, our method uses the P3 and P4 images from an extended source to account for the scattering of the cornea and the lens separately based on the computation of their contrasts.

The proposed methodology is in agreement with other techniques in terms of P4 contrast, which is the one comparable with the parameters given by the other instruments to account for the total scattered light [2,4–6,8,11]. Particularly, for eyes with cataracts very good correlations were found between the P4 contrast and the OSI/Log(S)/Densitometry (p<.001) despite the fact that the instruments are based on completely different principles. For eyes with corneal scattering, very good correlations were also shown between the P4 contrast and Log(S) (p<.001), and between the P4 contrast and OSI (p = 0.028). It should be noted that H and VH corneal scattering conditions corresponded to eyes wearing two CLs simultaneously. Differences in adaptation among patients, misalignments and heterogeneous tear distribution between CLs etc. might probably introduce aberrations that could affect the central part of the PSF and thus, the OSI. Moreover, densitometry was found to be useless in eyes wearing CLs as all values were of 100 (saturated).

On the other hand, we found that some cataracts (9 out of 16) affected the P3 contrast to some extent, since a ghost image appeared next to the P3 image. It should be highlighted that for one of the volunteers the P3 contrast could not be measured when simultaneously wearing two CLs due to a bad adaptation, which can probably explain the weaker correlation also found between the P3 contrast and the OSI in eyes with CLs.

In order to remove the dependency of the P3 contrast with the cataract when needed, a correction based on the maximum intensity of the ghost image was proposed. We hypothesize that the formation of a cataract involves a change in the refractive index inside the lens, e. g., generated at the interface between cortex and nucleus, which can produce internal reflections and result in the appearance of GPIs. Therefore, more than 4 Purkinje images are available in some cases although the additional ones are not so well delimited because the change in refractive index is not so abrupt; furthermore, they can partially overlap with the P3 image depending on the location of the cataract, affecting thus the P3 contrast value obtained.

In agreement with our findings, some authors have observed discontinuity zones using a Scheimpflug camera [20]. Castro and associates [21] have recently developed a swept-source optical coherent tomography SS-OCT able to characterize different features in the crystalline lens of older adults with and without a cataract. They concluded that the most common and notable opacity extended parallelly to either the anterior or posterior surface of the lens and that these surfaces were always hyperreflective. On the other hand, the roughness of the lens anterior surface has an age dependency, the well-known orange peel effect described by Navarro et al. [22], and this could also have an impact on the sharpness of P3 in some patients.

Although the results did not totally support the original hypothesis as P3 was also affected by light scattered in the lens in few cases, the methodology proposed is still valid if the correction of the GPI is used, i. e., in terms of P3′. Moreover, prior knowledge of the scattering source such as diagnosis of cataracts or corneal opacification is not required to apply our contrast-based methodology. Only if the image includes a GPI, the proposed correction is used to compute the P3′ contrast from the raw P3 value. This only happened in 9 out of 16 eyes with lenticular scattering and none of the eyes wearing scatter-customized CLs.

Finally, the method was found to be robust in a larger population of eyes with cataracts and corneal disorders. Accordingly, the technique can be very useful to measure the scattered light regardless its origin. In addition, it can discriminate where it comes from without the need of any previous diagnosis. Therefore, it might improve clinical practice as a complementary diagnostic tool in eyes with abnormally increased scattering such as cataracts or with corneal disorders. Future work will focus on the application of the developed methodology in a larger population of eyes, especially in eyes with cortical and subcapsular cataracts, to investigate if the GPI contribution removal is still valid in these cases. We

anticipate that both in research and clinical practice, this system will contribute to discriminate the origin of light scattering within the ocular structure, which remains elusive with current technology.

Disclosures

The authors have no conflicts of interest to declare.